

## Low Cost, High Speed Stereovision for Spatter Tracking in Laser Powder Bed Fusion

Christopher Barrett, Carolyn Carradero, Evan Harris,  
Jeremy McKnight, Jason Walker, Eric MacDonald, Brett Conner  
Youngstown State University, Youngstown, OH 44555

### Abstract

*Powder Bed Fusion Additive Manufacturing affords new design freedoms for metallic structures with complex geometries in high performance materials. The aerospace industry has identified the inherent benefits of AM not just in terms of shape creation but also with regard to producing replacement parts for an aging fleet of aircraft. However, for these parts to be deployed in flight-critical applications, the quality must be well established given the lack of flight heritage for the manufacturing process. As additive manufacturing is executed layerwise, opportunities exist to non-destructively verify the fabrication in situ with a qualify-as-you-go methodology. In this study, a pair of low cost, high speed cameras are integrated and synchronized together to provide stereovision in order to identify the size, speed, direction and age of spatter ejected from the laser melt pool. The driving hypothesis of the effort is that behavior of spatter can be reliably measured in order to determine the health of the laser process and ensure that spatter is not contaminating the build. Feasibility demonstrations are shown that describe how the measurements are made and characteristics calculated from the image data and how the data were verified with alternative measurements. Opportunities, future work and challenges are discussed.*

### 1.0 Introduction

Powder Bed Fusion (PBF) shows promise in the aerospace industry for providing complex structures fabricated with high performance metal alloys that are spatially tailored for both high performance and low weight. Interrelated assembly parts can now be consolidated into a single non-assembled structure with geometries not possible previously. However, in order to broaden industrial adoption in light of the high standards of the aerospace industry, evidence of the reliability of the fabricated structures will need to be collected in situ for each and every fabrication. Given the layer-by-layer processing with an unobstructed view of the top surface of the structure during fabrication, crucial aspects of the manufacturing process can be monitored in an unprecedented manner including the melt pool and ejecta. By characterizing this process and understanding the implications on process quality, a *qualify-as-you-go* methodology can be adopted as is required for insertion into manufacturing of flight critical hardware.

Within the taxonomy of PBF, Selective Laser Melting (SLM) has been optimized to create complex, high performance geometries in a diversity of metal alloys; however, process feedback is generally absent in production systems and is understood to remain as an eventual requirement for full qualification of these processes. Laser spatter is relatively well understood and can generally inform the process as to the quality of the structure under development. The final destination of the spatter after ejection can also have an impact on the fabrication through contamination or due to the introduction of irregular shaped and sized particles if the spatter returns back to either the melted section or open powder bed in the build chamber. The hypothesis of this work is that in situ monitoring using relatively low-cost cameras at relatively high-speed frames per second can provide data on the position and velocity of individual spatter and thus enable statistical analysis of general spatter behavior to improve quality and yield.

### 1.1 Previous Work of Others

Laser powder bed fusion is affected by several types of defects such as lack of fusion (Tang, Pistorius, and Beuth 2017), keyholing (King et al. 2014), balling (Khairallah et al. 2016), spatter (Criales et al. 2017), residual gas porosity (Cunningham et al. 2017), hatching strategy defects (Foster et al. 2015) and recoater defects (Foster et al. 2015). (Everton et al. 2016) provides an overview of in situ and nondestructive evaluation. The premise of this effort is that spatter should be ejected to the margins of the powder bed or outer shelves of the build chamber to ensure no problems and the spatter should not return to impact on an active top surface of the device in fabrication as the spatter is considered a contaminant. The particles are generally considered to be larger than feedstock powder, which can directly affect the quality of the manufacturing process by obstructed the laser melting at that point. Spatter particles ejected from the melt pool can land on the melted section and these particles can be much larger than the D90 size of the powder size distribution and negatively impact the subsequent layers (Criales et al. 2017; Khairallah et al. 2016; Christopher Barrett, Jason Walker, Rodrigo Enriquez Gutierrez, Eric MacDonald, Brett Conner 2018; Kneen 2016). Spatter can lead to other negative effects such as increasing surface roughness of a part (Mumtaz and Hopkinson 2009) or even increasing the layer thickness (Ladewig et al. 2016). Large spatter particles can cause damage to the recoater blade and the spatter particles might not melt during the subsequent laser pass (a process which is optimized for the smaller powder size feedstock). Even though the surrounding powder can melt, the large spatter can give rise to either unfused regions or create a cavity around the particle. Spatter can also land in unfused powder and change the local powder packing density and chemistry - either of which can affect melting behavior due to particle size differences.

In situ monitoring with the ultimate goal of providing feedback control has been researched in a variety of manners. (Taheri Andani et al. 2018, 2017; Repossini et al. 2017; Liu et al. 2015; Simonelli et al. 2015) all have explored the implications and behaviors of spatter in powder bed

fusion but none explored the use of high speed stereovision at the macro level to track the travel trends of spatter in the build chamber. Spatter in welding has also been explored and provides insights into AM spatter but it remains fundamentally different as the processes are not the same. (Craeghs et al. 2010); (Clijsters et al. 2014); (Lott et al. 2011); (Yadroitsev, Krakhmalev, and Yadroitsava 2014); (Doubenskaia et al. 2012); (Chivel 2013) all investigated monitoring the process at the melt pool by measuring the melt pool shape and temperature, and although the melt pool is the origin of spatter, this subject is outside of the scope of this work. The melt pool is the essence of SLM and clearly is critical to understanding the quality of a fabrication; (Kanko, Sibley, and Fraser 2016/5); (Krauss, Eschey, and Zaeh 2012); (Lane et al. 2016); (Bayle and Doubenskaia 2008); (Grasso et al. 2017) monitored and tracked the scan path which anecdotally has a significant impact on the amount and direction of spatter. This effort is intended to inform the process by identifying spatter behavior to determine if a build is compromised with the eventual goal of providing feedback for closed-loop control and a *qualify-as-you-go* paradigm.

High speed digital photography has been utilized to characterize spatter in several studies. Frame rates used include 1,000 fps (Repossini et al. 2017), 2000 fps (You, Gao, and Katayama 2014), 6000 fps (Taheri Andani et al. 2018) for laser additive processes. High speed thermal cameras have also been leveraged with frame rates of 1800 fps (Criales et al. 2017). High speed photography (3000 and 6000 fps) has also been used to characterize the behavior of interacting spatter for a multi-laser SLM 280 HL system (Taheri Andani et al. 2017).

The use of ultra high-speed imaging (100,000 frames per second) has uncovered that the mechanism causing spatter is from vapor driven entrainment of micro-particles by an ambient gas flow (Ly et al. 2017). Previously, it was believed that spatter was caused by laser induced recoil pressure (which is still true for laser welding processes, see (You, Gao, and Katayama 2014)). Ly et al. identified three distinct types of particles. The first involve particles with low vertical momentum that are carried into the melt pool. The second category of spatter particles have higher vertical momentum but originating more than 2 melt pool widths away from the beam and are carried into the trailing portion of the vapor jet. These are then ejected as cold particles. The third category of spatter particles are closer to the laser beam than the second category. These spatter particles are carried into the laser beam which heats the particles to the point of becoming incandescent, hot particles. With a scan speed of 1.5 m/s and laser of 200W and fusing stainless steel 316 powder, Ly et al. found that 60% of spatter particles observed are the third category (hot particle ejections) with velocities of 6–20 m/s and observed particle full width at half maximum (FWHM) diameters of 10 to 30 microns, another 25% are the second category (cold entrainment ejections) with velocities of 2–4 m/s and FWHM diameters of 20 to 30 microns, and the remaining

15% are recoil pressure induced droplet breakup ejections with velocities of 3–8 m/s and FWHM diameters of 15 to 70 microns. It should be noted that this work did not occur in a chamber with flowing inert gas (i.e. argon) over the powder bed as is common in most production systems. This inert gas flow could influence the flight path of the spatter particles.

## 2.0 Methods and Materials

The overarching goal of this effort is to statistically quantify the characteristics and behavior of spatter in order to identify strategies to mitigate any resulting reductions in quality. A secondary consideration is to implement a system that was less than 5% of the total cost of the manufacturing system to broaden the adoption of the proposed monitoring system. For stereo analysis, calibration and camera mount design are critical parameters for accuracy in measurements.

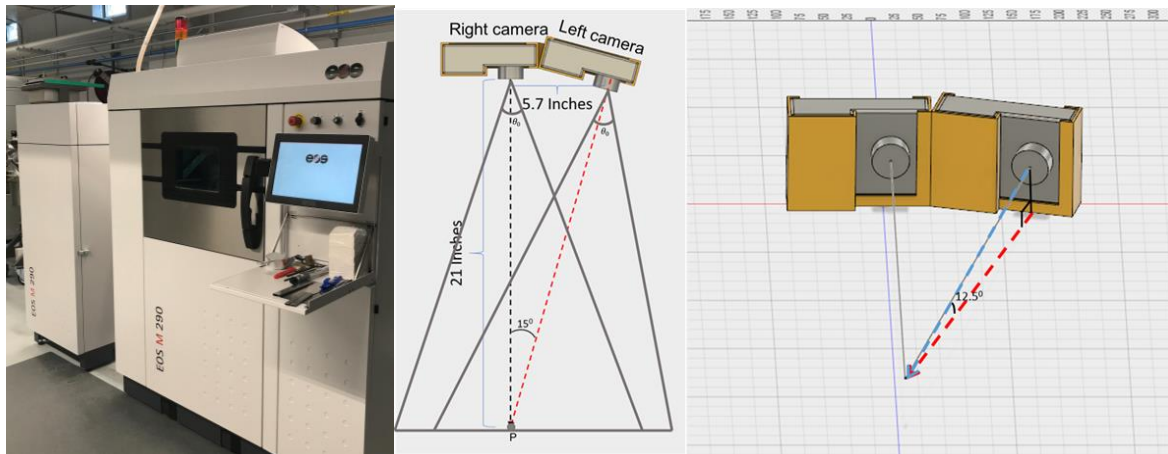


**Figure 1** - EOS M290 with front port window (left) and stereovision schematic (right)

### 2.1 High speed stereovision camera system

Two low cost, high speed cameras (FPS1000 by The Slow Motion Camera Company) were purchased and integrated together in a stiff housing in order to minimize any movement relative between the cameras, and thereby allowing for standardization during calibration and live spatter measurements. An 18 mm lens was used with an aperture of f 4.5 (to increase depth of field). Images were taken in raw with a 1280x720 pixel count (maximum allowed for the camera). Calculating the spatial resolution for visible light (470 nm – 625 nm) gives a range of 18  $\mu\text{m}/\text{pixel}$  to 24  $\mu\text{m}/\text{pixel}$ .

## 2.2 Stereovision and Epipolar Geometry to identify position and direction of spatter

For calibration, the intrinsic parameters include information on the camera calibration matrix (K) and distortion coefficients which are obtained through single camera calibration. The former is given by

$$K = \begin{bmatrix} f_x & 0 & c_x \\ 0 & f_y & c_y \\ 0 & 0 & 1 \end{bmatrix} \quad \text{eq. 1}$$

$$K' = \begin{bmatrix} f_x' & 0 & c_x' \\ 0 & f_y' & c_y' \\ 0 & 0 & 1 \end{bmatrix} \quad \text{eq. 2}$$

where K and K' are camera calibration matrices,  $f_x$ ,  $f_x'$ ,  $f_y$ ,  $f_y'$  are focal length in pixel units,  $c_x$ ,  $c_x'$ ,  $c_y$  and  $c_y'$  are principal points, normally at the center of the image. The open source Computer Vision library was used to locate a checkerboard pattern in fifty different poses (fig. 2). The intrinsic parameters are then used during stereo calibration, where coincident images from a stereo pair determine the extrinsic parameters of the system. The extrinsic parameters correspond to the rotation (R) and translation (t) between the two cameras,

$$P = K[I|0] \quad \text{eq. 3}$$

$$P' = K'[R|t] \quad \text{eq. 4}$$

where P and P' are the projection matrices which are 3x4 matrices, I is the identity matrix, R is the rotation matrix and t is the translation matrix. The matrices returned from calibration are then used to rectify simultaneous frames using the OpenCV function stereoRectify. Rectification calculates the necessary values to apply a geometric transformation on both images, ideally resulting in near horizontal epipoles on the image plane. The projection matrices were then used to triangulate two matched points between simultaneous frames. This method could then be applied to measure the length of light exposure caused by spatter between two sequential frames.

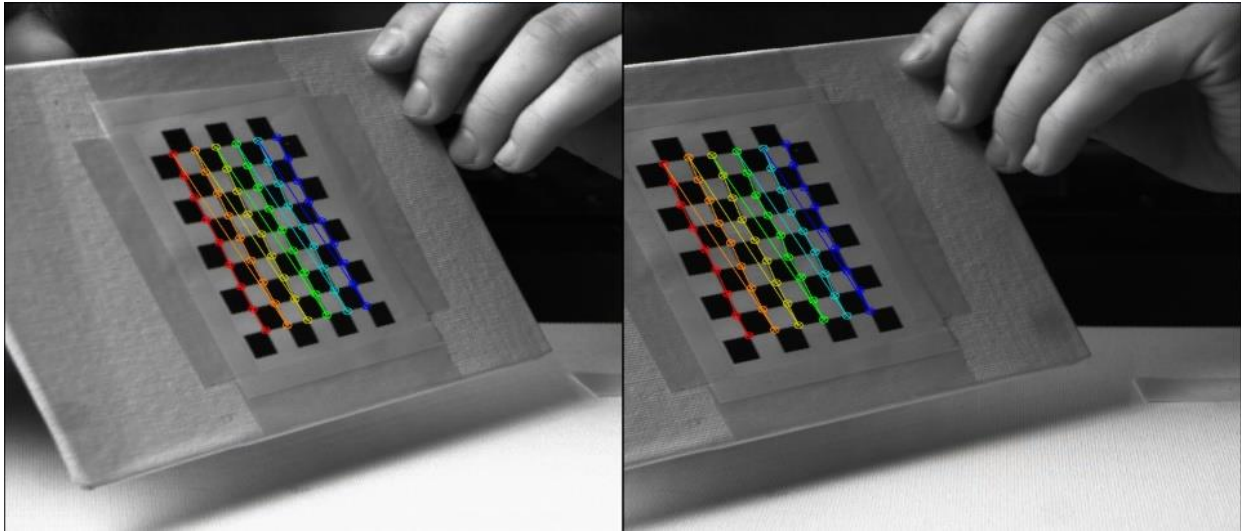


**Figure 2** - Stereo Calibration between two coincident images from different perspectives.

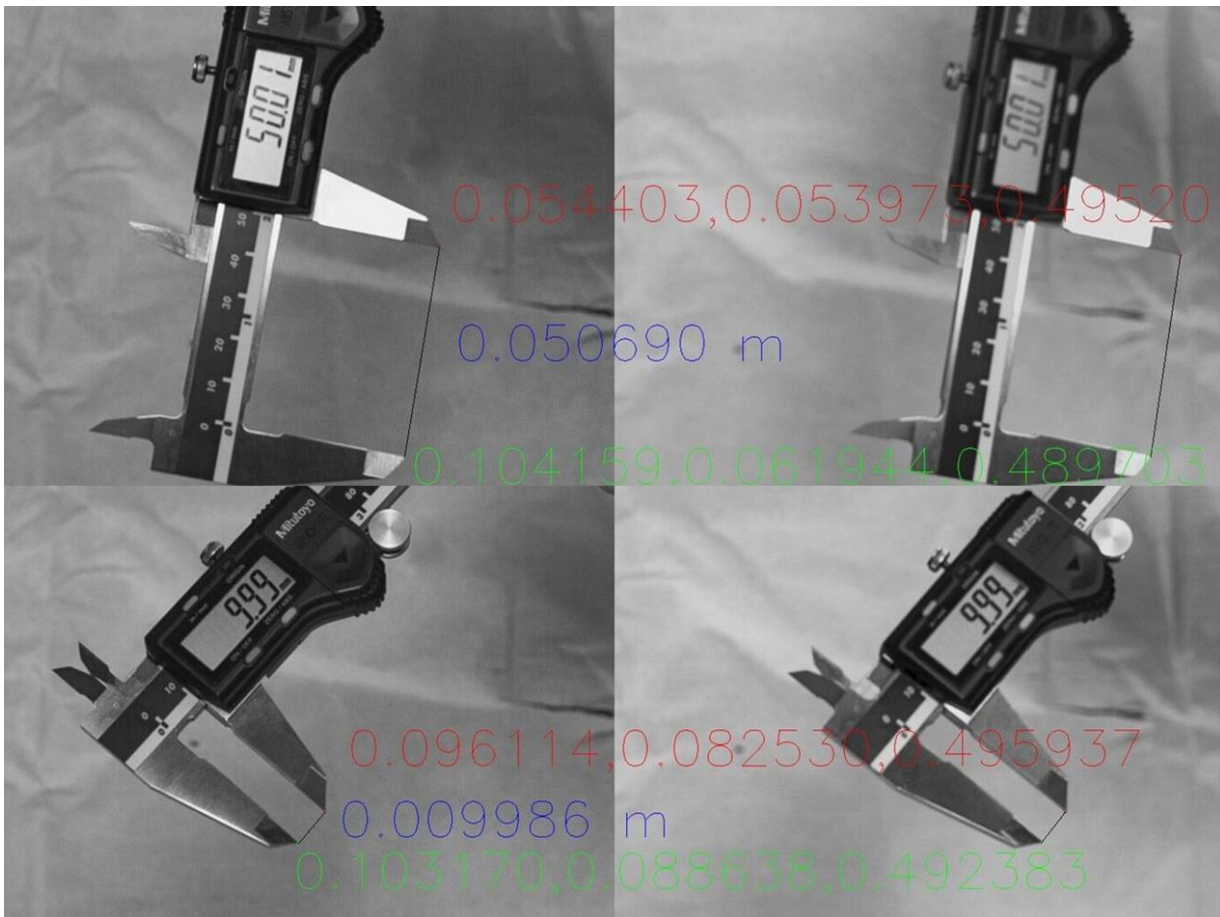


**Figure 3** - Stereovision quality assurance using a caliper (50.01 mm top, 9.99 mm bottom).

Two stereo images of a caliper were taken as a calibration check (fig. 3), two points were found, and the distance between them was measured. The distance of the first measurement between the two points in the caliper was 50.01 mm, while the distance measured with stereovision was 50.69 mm, producing an error of 1.34%. The second distance was 9.99 mm, while the measured stereovision distance was 9.986 mm producing an error of 0.04% (which is precise as it is below the accuracy of the caliper).

### 3.0 Results and Discussion

A selective laser melting (SLM) build was completed with the camera system outside the front port of an EOS M290. Ideally the system would be housed within the build chamber to provide the closest perspective which allowed for the entire build volume to be seen from both cameras; however, in this preliminary study, an external perspective provided benefits such as physical access to the cameras, etc. Future work will include integrating the camera system more closely to the powder bed in a final system which is planned to be installed in a 3D Systems ProX 320 where internal integration will be eased with the larger build volume. Some concern exists regarding the vacuum pulled temporarily at the beginning of the build and the impact that this may have on the health of the electronics. Eventually, data collected from both of the two systems (ProX 320 and M290) will allow for a comparison of spatter behavior across a diversity of processes.

#### 3.1 Sequential versus single image spatter tracking

To validate the concept of using over-exposure to integrate the light and identify the speed and direction of the spatter from a single stereovision image, some spatter particles were tracked for multiple frames as an alternative method of measuring velocity and to determine how the velocity and direction changed over a larger time frame (3 mS rather than 0.5 mS). As the exposure was 500  $\mu$ s and the period of the imaging was 1 mS, the distance traveled from frame to frame was expected to be twice the distance of the length of the spatter line in any given frame - minus the effects of gravity or build chamber atmosphere. In fig. 4, three distinct spatter particles are tracked across three sequential frames as shown on the bottom of the figure. The top of the figure shows the three frames overlaid on each other with green (frame 1), blue (frame 2) and red (frame 3) coloring to distinguish the particles in time. As the period of the image acquisition (1000 fps frequency, 1000  $\mu$ s period) is twice as long as the exposure time (500  $\mu$ s), the smeared images for each of the three cases should have similar lengths and the lines should be separated by the same length - as the camera exposure duty cycle is 50% (500  $\mu$ s exposure with 1000  $\mu$ s imaging). This is shown to be true not just for the two fast particles ejected to the right but also for the older and slower particle to the left (see Table 1). The process emission is also shown as a nebulous form at the bottom of each frame and is in fact moving along the laser path as expected. Other noise is shown primarily in the third red frame. As the third frame has the faintest spatter signature due to the age of the particles, the threshold for detection was reduced and this introduced significant

noise into this frame. By attempting to capture only one image per spatter and ignoring very new and very old spatter, the problem of uniform brightness is expected to be eliminated for the automated computer script by capturing only a narrow band of brightness which in turn results in only a certain age of spatter being captured in the computer vision.

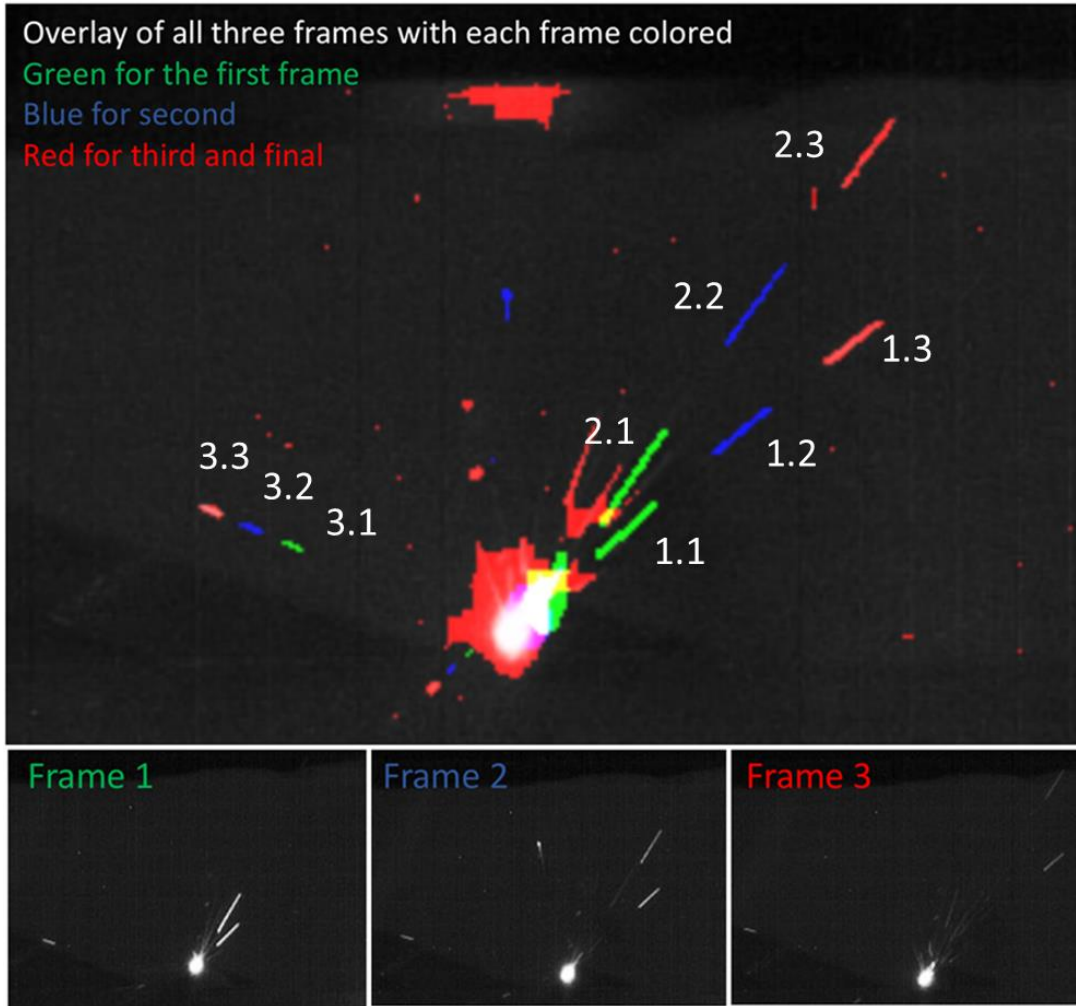


**Figure 4** - Sequential imaging of the right camera to demonstrate that tracked spatter measurements (frame to frame with an overlay) can be obtained in a single image.

### 3.2 Stereo imaging of spatter and determination of velocity and direction

To demonstrate the spatter monitoring approach, fig. 5 shows a single dual-frame capture of an instance of significant spatter production ejected from the melt pool. In both cameras, three spatter particles are shown and easily matched between the two cameras. OpenCV computer vision identifies these regions as high intensity (white) and with a large aspect ratio forming a line that projects back to the melt pool as expected. In each spatter case, the length of the image artifact is an overexposure across 500  $\mu$ s and thus provides the distance traveled over that time and

consequently a velocity can be calculated. The particles are expected to follow a normal ballistic trajectory and change their velocity with time and drag; however, this is assumed negligible over the short 500  $\mu\text{s}$  time frame. Each spatter can be identified by two points: the beginning and the end. For each point in each image, a row and column can be determined. With the same feature (e.g. start or end of spatter streak) as seen in two images, four values (rows and columns) can be obtained and through epipolar geometry the location of the point in 3D space (X, Y, and Z coordinates) can be determined. With the 3D location of both the start and stop of the spatter, a direction vector can be generated and the magnitude of the vector (length in mm) can be divided by the 500  $\mu\text{s}$  exposure time to calculate a velocity. Furthermore, if the beginning of the spatter and the melt pool are known in 3D space, a distance can be calculated from the origin (the melt pool) to the spatter streak beginning. By dividing the distance by the velocity, an age can be established for the particle. The older the particle, the less bright the emissions. This monotonically decreasing brightness is a characteristic that is leveraged to limit the image identification of the spatter to only one time and to avoid double or multiple counting in statistical evaluation. Spatter that are too bright (often in the process of formation or calving and therefore without a distinct start and stop), and conversely, those that are not sufficiently bright will be excluded. The intent is for the computer vision system to only identify the spatter once in its lifecycle to collect accurate statistical data on position and velocity and to avoid the challenging tracking of the particle between frames. Some particles are much faster than others so separation between the same particle on two sequential frames can vary significantly. Moreover, the brightness of the particle is ephemeral and identifying spatter on two frames may not always be possible. Fig. 5 shows both the left and right-side cameras of an active moment during selective laser melting of powder with substantial generation of spatter. Table 1 shows the X, Y, Z direction and velocity of each of the spatter shown in figure 4.

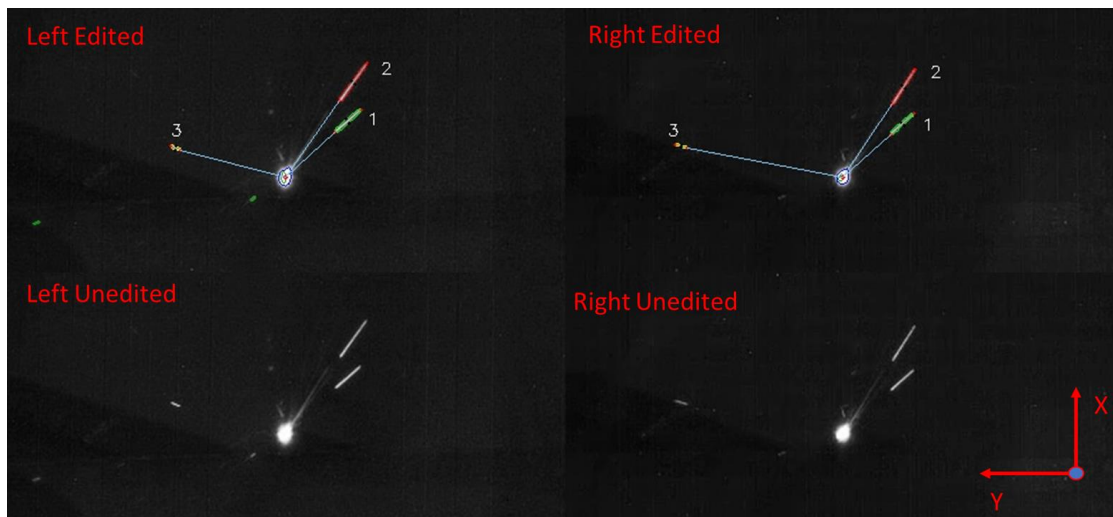


**Figure 5:** Stereovision imaging of spatter of varying directions and speeds (+Z into plane)

**Table 1:** Spatter from fig. 5 described in direction, velocity

Particle	Start ([x,y,z], mm)	End ([x,y,z], mm)	Direction ([x,y,z], mm)	Velocity (m/s)
1.1	[0.6590, -7.590, 3.301]	[2.875, -10.20, 6.840]	[2.216, 2.610, 3.539]	9.85
1.2	[3.025, -10.40, 6.017]	[5.249, -12.80, 9.481]	[2.223, 2.392, 3.463]	9.52
1.3	[5.182, -13.21, 8.668]	[7.160, -15.17, 12.85]	[1.978, 1.960, 3.463]	10.05
Avg Particle 1				9.81
2.1	[2.415, -7.800, 3.881]	[6.730, -10.21, 8.902]	[4.315, 2.410, 5.021]	14.09
2.2	[6.730, -10.21, 8.902]	[10.62, -12.39, 13.70]	[3.893, 2.176, 4.802]	13.11
2.3	[10.62, -12.39, 13.70]	[14.49, -15.15, 16.85]	[3.866, 2.768, 3.141]	11.40
Avg Particle 2				12.87
3.1	[-0.650, 19.04, 19.16]	[-0.305, 20.65, 20.36]	[0.3452, 1.604, 1.198]	4.06
3.2	[-0.4195, 20.98, 21.06]	[0.1509, 22.43, 21.51]	[0.5704, 1.451, 0.4597]	3.25
3.3	[0.1509, 22.43, 21.52]	[0.1678, 24.66, 24.05]	[0.01691, 2.227, 2.535]	6.75
Avg Particle 3				4.69

Future work will investigate more accurately where in the melt pool each spatter originated and furthermore, if the melt pool motion (build path) has an impact on the quantity, speed and direction of the spatter. Preliminarily it can be noted that when the laser changes direction, the production of spatter dramatically increases and the spatter tends to favor the direction opposite to the new laser scan path. The ultimate goal of this research effort is (1) to automate the one detection of each spatter and to collect statistical data over millions of frames (2) to verify that by determining the position and velocity of the spatter just after creation that this method can predict the final impact destination of the spatter in order to improve quality and yield.

### 3.3 Spatter calving and implications on melt pool location and contour determination

On a large fraction of the captured images, spatter was shown in the nascent stage - still connected with the melt pool. Fig. 6 shows the extreme case of a new particle which has yet to fully emerge from the melt pool and is being “calved”. Consequently, the velocity and age of the particle cannot be determined as there is no start point other than the melt pool which is large and provides an insufficient data as to the exact origination. These cases are therefore ignored with the understanding that as the spatter emerges completely, the particle will be captured and evaluated in a subsequent frame. An additional technique to avoid evaluating calving spatter is to identify and contour the melt pool. If excessive concavity exists (easily detectable in OpenCV), the contour can be ignored. Furthermore, if the centroid of the melt pool is calculated as required in order to determine the origin in an age calculation, the centroid can be adjusted to eliminate skewing of the location based on calving spatter influence.



**Figure 6** - Spatter calving where new spatter particles have been formed and are being ejected.

These “half-baked” spatter do not have a distinct start and stop point which means that although the direction can be determined, the velocity cannot. Furthermore, the centroid of the melt pool is distorted and incorrectly pulled to the side of calving particle.

#### 4.0 Conclusions

In conclusion, this paper details a low-cost method for spatter tracking and analysis for laser powder bed fusion. The key completed objectives are as follows:

- Stereovision demonstrates a reliable way to gather in situ statistical information about spatter particles.
- Spatter Age, Velocity, Direction, and Size have been reliably measured.
- Low cost (less than \$10,000 USD) and open source resources were successfully used to accomplish this work.
- The foundation for an automated system has been laid, which will allow for the gathering of statistical data for future analysis.

Future work will entail the automation and statistical identification of trends which can be used for defect analysis in laser powder bed fusion.

#### Acknowledgments

We would like to thank the Friedman Endowment for Manufacturing at Youngstown State University. This effort was performed in part through the National Center for Defense Manufacturing and Machining under the America Makes Program entitled “Maturation of Advanced Manufacturing for Low Cost Sustainment (MAMLS)” and is based on research sponsored by Air Force Research Laboratory under agreement number FA8650-16-2-5700. The U.S. Government is authorized to reproduce and distribute reprints for Governmental purposes notwithstanding any copyright notation thereon.

## References

- Bayle, F., and M. Doubenskaia. 2008. "Selective Laser Melting Process Monitoring with High Speed Infra-Red Camera and Pyrometer." In *Fundamentals of Laser Assisted Micro- and Nanotechnologies*, 698505–698505 – 8. International Society for Optics and Photonics.
- Chivel, Y. 2013. "Optical In-Process Temperature Monitoring of Selective Laser Melting." *Physics Procedia* 41: 904–10.
- Christopher Barrett, Jason Walker, Rodrigo Enriquez Gutierrez, Eric MacDonald, Brett Conner. 2018. "A Low Cost, High-Speed Optical Monitoring System for Tracking Spatter During Laser Powder Bed Fusion." presented at the TMS 2018, Phoenix, AZ, March.
- Clijsters, S., T. Craeghs, S. Buls, K. Kempen, and J-P Kruth. 2014. "In Situ Quality Control of the Selective Laser Melting Process Using a High-Speed, Real-Time Melt Pool Monitoring System." *International Journal of Advanced Manufacturing Technology* 75 (5-8): 1089–1101.
- Craeghs, Tom, Florian Bechmann, Sebastian Berumen, and Jean-Pierre Kruth. 2010. "Feedback Control of Layerwise Laser Melting Using Optical Sensors." *Physics Procedia* 5, Part B: 505–14.
- Criales, Luis E., Yiğit M. Arsoy, Brandon Lane, Shawn Moylan, Alkan Donmez, and Tuğrul Özel. 2017. "Laser Powder Bed Fusion of Nickel Alloy 625: Experimental Investigations of Effects of Process Parameters on Melt Pool Size and Shape with Spatter Analysis." *International Journal of Machine Tools & Manufacture* 121 (October): 22–36.
- Cunningham, Ross, Sneha P. Narra, Colt Montgomery, Jack Beuth, and A. D. Rollett. 2017. "Synchrotron-Based X-Ray Microtomography Characterization of the Effect of Processing Variables on Porosity Formation in Laser Power-Bed Additive Manufacturing of Ti-6Al-4V." *JOM Journal of the Minerals Metals and Materials Society* 69 (3): 479–84.
- Doubenskaia, M., M. Pavlov, S. Grigoriev, E. Tikhonova, and I. Smurov. 2012. "Comprehensive Optical Monitoring of Selective Laser Melting." *Journal of Laser Micro Nanoengineering* 7 (3): 236–43.
- Everton, Sarah K., Matthias Hirsch, Petros Stravroulakis, Richard K. Leach, and Adam T. Clare. 2016. "Review of in-Situ Process Monitoring and in-Situ Metrology for Metal Additive Manufacturing." *Materials & Design* 95 (April): 431–45.
- Foster, B. K., E. W. Reutzel, A. R. Nassar, B. T. Hall, S. W. Brown, and C. J. Dickman. 2015. "Optical, Layerwise Monitoring of Powder Bed Fusion." In *Solid Freedom Fabrication Symp. Proc.* <https://sffsymposium.engr.utexas.edu/sites/default/files/2015/2015-24-Foster.pdf>.
- Grasso, Marco, Vittorio Laguzza, Quirico Semeraro, and Bianca Maria Colosimo. 2017. "In-Process Monitoring of Selective Laser Melting: Spatial Detection of Defects Via Image Data Analysis." *Journal of Manufacturing Science and Engineering* 139 (5): 051001.
- Kanko, Jordan A., Allison P. Sibley, and James M. Fraser. 2016/5. "In Situ Morphology-Based Defect Detection of Selective Laser Melting through Inline Coherent Imaging." *Journal of Materials Processing Technology* 231: 488–500.
- Khairallah, Saad A., Andrew T. Anderson, Alexander Rubenchik, and Wayne E. King. 2016. "Laser Powder-Bed Fusion Additive Manufacturing: Physics of Complex Melt Flow and Formation Mechanisms of Pores, Spatter, and Denudation Zones." *Acta Materialia* 108 (April): 36–45.
- King, Wayne E., Holly D. Barth, Victor M. Castillo, Gilbert F. Gallegos, John W. Gibbs, Douglas E. Hahn, Chandrika Kamath, and Alexander M. Rubenchik. 2014. "Observation of Keyhole-Mode Laser Melting in Laser Powder-Bed Fusion Additive Manufacturing." *Journal of Materials Processing Technology* 214 (12): 2915–25.
- Kneen, Travis J. 2016. "Characterizing the High Strain Rate Mechanical Behavior of Stainless Steel 316L Processed by Selective Laser Melting." Youngstown State University.
- Krauss, H., C. Eschey, and M. Zaeh. 2012. "Thermography for Monitoring the Selective Laser Melting

- Process.” In *Proceedings of the Solid Freeform Fabrication Symposium*.  
<http://sffsymposium.engr.utexas.edu/Manuscripts/2012/2012-76-Krauss.pdf>.
- Ladewig, Alexander, Georg Schlick, Maximilian Fisser, Volker Schulze, and Uwe Glatzel. 2016. “Influence of the Shielding Gas Flow on the Removal of Process by-Products in the Selective Laser Melting Process.” *Additive Manufacturing* 10 (April): 1–9.
- Lane, Brandon, Shawn Moylan, Eric Whitenton, and Li Ma. 2016. “Thermographic Measurements of the Commercial Laser Powder Bed Fusion Process at NIST.” *Rapid Prototyping Journal* 22 (5): 778–87.
- Liu, Yang, Yongqiang Yang, Shuzhen Mai, Di Wang, and Changhui Song. 2015. “Investigation into Spatter Behavior during Selective Laser Melting of AISI 316L Stainless Steel Powder.” *Materials & Design* 87 (December): 797–806.
- Lott, Philipp, Henrich Schleifenbaum, Wilhelm Meiners, Konrad Wissenbach, Christian Hinke, and Jan Bültmann. 2011. “Design of an Optical System for the In Situ Process Monitoring of Selective Laser Melting (SLM).” *Physics Procedia* 12, Part A: 683–90.
- Ly, Sonny, Alexander M. Rubenchik, Saad A. Khairallah, Gabe Guss, and Manyalibo J. Matthews. 2017. “Metal Vapor Micro-Jet Controls Material Redistribution in Laser Powder Bed Fusion Additive Manufacturing.” *Scientific Reports* 7 (1): 4085.
- Mumtaz, Kamran, and Neil Hopkinson. 2009. “Top Surface and Side Roughness of Inconel 625 Parts Processed Using Selective Laser Melting.” *Rapid Prototyping Journal* 15 (2): 96–103.
- Repossini, Giulia, Vittorio Laguzza, Marco Grasso, and Bianca Maria Colosimo. 2017. “On the Use of Spatter Signature for in-Situ Monitoring of Laser Powder Bed Fusion.” *Additive Manufacturing* 16 (August): 35–48.
- Simonelli, Marco, Chris Tuck, Nesma T. Aboulkhair, Ian Maskery, Ian Ashcroft, Ricky D. Wildman, and Richard Hague. 2015. “A Study on the Laser Spatter and the Oxidation Reactions During Selective Laser Melting of 316L Stainless Steel, Al-Si10-Mg, and Ti-6Al-4V.” *Metallurgical and Materials Transactions A* 46 (9): 3842–51.
- Taheri Andani, Mohsen, Reza Dehghani, Mohammad Reza Karamooz-Ravari, Reza Mirzaeifar, and Jun Ni. 2017. “Spatter Formation in Selective Laser Melting Process Using Multi-Laser Technology.” *Materials & Design* 131 (October): 460–69.
- . 2018. “A Study on the Effect of Energy Input on Spatter Particles Creation during Selective Laser Melting Process.” *Additive Manufacturing* 20 (March): 33–43.
- Tang, Ming, P. Chris Pistorius, and Jack L. Beuth. 2017. “Prediction of Lack-of-Fusion Porosity for Powder Bed Fusion.” *Additive Manufacturing* 14 (March): 39–48.
- Yadroitsev, I., P. Krakhmalev, and I. Yadroitsava. 2014. “Selective Laser Melting of Ti6Al4V Alloy for Biomedical Applications: Temperature Monitoring and Microstructural Evolution.” *Journal of Alloys and Compounds* 583 (January): 404–9.
- You, Deyong, Xiangdong Gao, and Seiji Katayama. 2014. “Monitoring of High-Power Laser Welding Using High-Speed Photographing and Image Processing.” *Mechanical Systems and Signal Processing* 49 (1–2): 39–52.
- Donaldson, Brent. 2017. “Can Topography Scans Redraw the Metal Additive Inspection Map?” *Additive Manufacturing* [Blog Post]. Retrieved from URL <https://www.additivemanufacturing.media/blog/post/can-topography-scans-redraw-the-metal-additive-inspection-map/>. (December 1).
- Foster, B. K., Reutzler, E. W., Nassar, A. R., Hall, B. T., Brown, S. W., & Dickman, C. J. (2015). Optical, layerwise monitoring of powder bed fusion. In *Solid Free. Fabr. Symp. Proc* (pp. 295-307).